

A COMPARISON OF $\omega - k$ AND GENERALIZED SAR INVERSION FOR RUNWAY IMAGING

Nail Çadallı and David C. Munson, Jr.

Coordinated Science Laboratory,
University of Illinois, Urbana, IL, 61801
e-mail: cadalli@dsp.csl.uiuc.edu, munson@dsp.csl.uiuc.edu

ABSTRACT

Wavefront curvature must be taken into account in highly squinted SAR applications, such as runway imaging from an aircraft approaching for landing. The $\omega - k$ algorithm, which successfully incorporates wavefront curvature into the processing, shows certain aberrations in the highly squinted case, depending on the accuracy of the interpolation and the location of the targets in the scene. An alternative SAR inversion method performs a more general basis decomposition of the imaging kernel in order to accurately model the wavefront curvature. This general inversion method is inherently robust to noise, however, it is computationally much more expensive. The performance of the $\omega - k$ algorithm can be improved by increasing the computational load only linearly [1]. Here we make a fair comparison of the two methods, where they are constrained to use the same amount of computation.

1. INTRODUCTION

Synthetic Aperture Radar (SAR) is used to produce high-resolution radar imagery [2]. SAR typically employs a plane-wave approximation of the wavefront. However, in some cases, including in runway imaging from an approaching aircraft, wavefront curvature must be taken into account [3]. The so-called $\omega - k$ algorithm increases resolution by accurately modeling the actual spherical wave [4, 5]. In runway imaging, the radar looks almost straight ahead, which makes the squint angle close to 90 degrees. In such a high-squint-angle case, the $\omega - k$ algorithm shows certain aberrations depending on the location of the target in the scene and accuracy of the interpolation. Based on our analysis of the $\omega - k$ algorithm, we have found out that the accuracy of the interpolation, and hence the overall image quality, can be improved simply by increasing the number of temporal samples in the collected data [1]. This increases the overall computational complexity only linearly in the number of temporal samples.

Even though it is computationally attractive, the $\omega - k$ algorithm may not be the optimal way to solve the highly squinted SAR imaging problem. We, therefore, consider using another algorithm that accurately models the wavefront curvature. This method is a general inversion algorithm which has been suggested for the numerical solution of the Fredholm integral equation of the first kind [6]. It was originally applied to borehole induction measurements, and has been formulated for SAR inversion as well [7]. We will refer to this approach as the general inversion method (GIM). The $\omega - k$ algorithm decomposes the imaging kernel in a Fourier basis, while GIM makes a similar decomposition in a more general orthogonal basis. This enables a better representation of the data.

Hence, GIM is expected to produce reconstructions with less severe aberrations that depend on the location of the target in the scene. Furthermore, the method is inherently robust to measurement noise. However, this general decomposition brings a heavy computational burden.

Both the $\omega - k$ algorithm and GIM have been suggested for imaging a runway from an approaching aircraft during landing in order to determine whether there is any object either on or near the runway that would make the landing unsafe [8]. In this study, our objective is to make a comparison between the image reconstruction performances of the $\omega - k$ algorithm and GIM for the runway imaging scenario where the squint angle is close to 90 degrees. Since the performance of the $\omega - k$ algorithm can be improved by a linear increase in the amount of computation, a fair comparison of the two methods involves allowing the $\omega - k$ algorithm to use as many computations as GIM uses. In the following, we describe the data model and briefly explain both of the methods before we present the simulation results and discussion.

2. DATA MODEL AND $\omega - k$ PROCESSING

Figure 1 describes the geometry of the data collection scenario in the ground plane. The radar platform is an aircraft approaching a runway for landing. The runway lies along the y axis straight ahead of the aircraft. The elevation of the aircraft is omitted in the following but the generalization of the data model to slant range geometry is straightforward. The squint angle γ_0 of the scene center (X_0, Y_0) with respect to the origin of the coordinate system is typically close to 90 degrees. At regular spatial intervals along the synthetic aperture, the radar transmits a pulse and collects the return. The transmitted signal is the real part of the pass-band signal $s_T(t) = p(t) \exp(j\omega_0 t)$. For a linear FM pulse, $p(t) = \exp(j\alpha t^2)$ for $|t| \leq \tau_p/2$ and zero otherwise. Here $\omega_0 = 2\pi f_0$ is the angular center frequency of the chirp signal and 2α is the chirp rate. Deramping the return signal yields, after omitting known and negligible terms (see [1] for details),

$$s(\omega, y) = \iint_{-\infty}^{\infty} g(x', y') f(x', y - y'; \omega) dx' dy' \quad (1)$$

where $f(x', y; \omega) = \exp(j2kr(x', y))$ is the *imaging kernel*. The range function is given as $r(x', y) = [x'^2 + y^2]^{\frac{1}{2}}$ when the radar is at location y on the flight path and the coordinates of a particular scatterer are given by (x', y') . The wavenumber is given by $k = \omega/c$, where $\omega = \omega_0 + 2\alpha(t - \tau_0)$ with $\tau_0 = \frac{2R_0}{c}$ and R_0

being the distance from the origin of the coordinate system to the center of the target scene. We assume that the scene area is illuminated uniformly within the range of observation angles and $g(x, y)$ vanishes outside the scene area. Representing the imag-

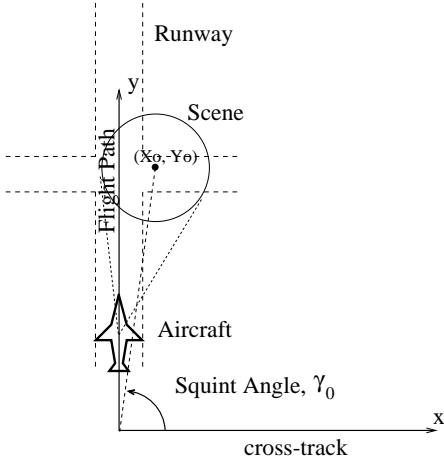


Fig. 1. Geometry of SAR data collection for runway imaging.

ing kernel by its approximate Fourier transform yields, (see [1] and references therein), $S(\omega, k_y) \approx A G(\sqrt{4k^2 - k_y^2}, k_y)$ where $S(\omega, k_y)$ is the one-dimensional Fourier transform of $s(\omega, y)$ and $G(k_x, k_y)$ is the two-dimensional Fourier transform of $g(x, y)$. A is a complex constant. Taking the two-dimensional inverse Fourier transform gives the reflectivity function. However, as indicated by the relation between k_y and $k_x = [4k^2 - k_y^2]^{\frac{1}{2}}$, the Fourier data lies on an irregular grid. Thus, interpolation of the data onto a Cartesian grid is necessary before a two-dimensional inverse fast Fourier transform. The $\omega - k$ image formation algorithm is summarized in Figure 2. In the first phase multiplication, k_y^c is the center frequency of the data in the y dimension. This phase shift in the spatial domain causes the k_y spectrum of the data to be shifted to baseband. The second phase multiplication in the wavenumber domain shifts the spatial-domain data such that the center of the reconstructed image is the scene center.

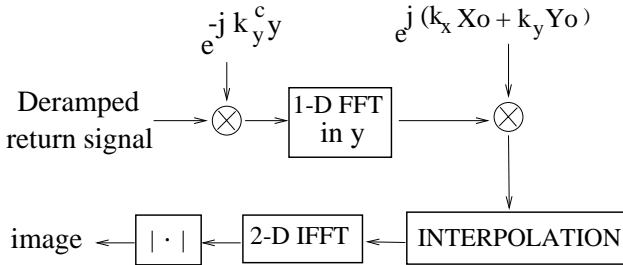


Fig. 2. Block diagram of $\omega - k$ algorithm.

The Fourier data, in the $k_x - k_y$ plane, lies on arcs which are parts of concentric circles between radial lines determined by the extremes of the squint angles. We have shown in [1] that as the number of the temporal samples is increased, the interpolation from this circular grid to a Cartesian grid becomes more accurate, resulting in better reconstructions.

3. GENERALIZED SAR INVERSION

Performing range compression on the quadrature demodulated return signal we have the return signal in spatial coordinates as

$$s(x, y) = \iint_{-\infty}^{\infty} K(x, y - y'; x') g(x', y') dx' dy'. \quad (2)$$

The *measurement kernel* is given as

$$K(x, y; x') = \rho \left(\frac{2(x - r(x', y))}{c} \right) e^{-j2k_0 r(x', y)}, \quad (3)$$

where $k_0 = \omega_0/c$ and $\rho(t)$ is the autocorrelation of the pulse $p(t)$. The expression for the range compressed signal is now in the form of Fredholm integral equation of the first kind with a nonseparable kernel. The imaging method described in [6] can be applied to this case as given in [7] and is briefly summarized in the following in order to point out later the computational requirements in each step.

First we decompose (2) into a set of integral equations each along a basis component of the x-range space of the measurement kernel. For this purpose, we first find a basis for this subspace and then project the measurements onto each basis component. Let this basis be composed of vectors $\{\gamma_i(x)\}_{i=1}^I$. Then form the product

$$\Gamma(x, z) = \iint_{-\infty}^{\infty} K(x, y'; x') K^*(z, y'; x') dx' dy'. \quad (4)$$

Basis functions $\{\gamma_i(x)\}_{i=1}^I$ can be obtained by eigendecomposition of the discrete version of $\Gamma(x, z)$. This is a spectral representation of the measurement kernel. The number of basis functions, I , is determined by an energy constraint on the singular values of the discrete form of $\Gamma(x, z)$. For instance, in our simulations we choose I to keep 99% of the energy. We project the measurements and the measurement kernel onto the subspace spanned by $\{\gamma_i(x)\}_{i=1}^I$ as

$$f_i(y) = \int_{-\infty}^{\infty} \gamma_i^*(x) s_2(x, y) dx \quad (5)$$

$$K_i(y, x') = \int_{-\infty}^{\infty} \gamma_i^*(x) K(x, y; x') dx \quad (6)$$

and obtain the decomposition into projected measurements as

$$f_i(y) = \iint_{-\infty}^{\infty} K_i(y - y', x') g(x', y') dx' dy'. \quad (7)$$

Approximating the kernel by $K_i(y, x') \approx \sum_{j=1}^{J_i} \lambda_{ij} u_{ij}(y) v_{ij}^*(x')$, the integral can be represented in multichannel convolution form. Let $\{q_m(x')\}_{m=1}^M$ be an orthonormal basis for the space spanned by $v_{ij}(x')$ for $i = 1, \dots, I, j = 1, \dots, J_i$. Then, $v_{ij}(x') = \sum_{m=1}^M \alpha_{ijm} q_m(x')$ and we have

$$f_i(y) \approx \sum_{m=1}^M \int_{-\infty}^{\infty} z_{im}(y - y') p_m(y') dy' \quad (8)$$

where

$$z_{im}(y) = \sum_{j=1}^{J_i} \lambda_{ij} u_{ij}(y) \alpha_{ijm}^* \quad (9)$$

$$p_m(y') = \int_{-\infty}^{\infty} q_m^*(x') g(x', y') dx'. \quad (10)$$

Solving the multichannel deconvolution problem, we obtain the estimate of the projections as

$$\hat{p}_m(y') = \sum_{i=1}^I \int_{-\infty}^{\infty} h_{mi}(y' - y) f_i(y) dy. \quad (11)$$

The deconvolution filters $h_{mi}(y)$ can be obtained by an inversion scheme such as regularized least squares. Then back-projection yields the estimate of the reflectivity:

$$\hat{g}(x', y') = \sum_{m=1}^M \hat{p}_m(y') q_m(x'). \quad (12)$$

4. SIMULATIONS AND DISCUSSION

Here, we compare the reconstruction performance of the two methods under the condition that the $\omega - k$ and GIM algorithms use the same number of computations. Therefore, we first elaborate on the computational cost of the methods. The computational complexity of the $\omega - k$ algorithm can be easily calculated from Figure 2. We have $N_\omega \times N_y$ samples of the return signal, $s(\omega, y)$. The Cartesian interpolation grid consists of $N_x \times N_y$ points. In the interpolation step, the number of multiplications is at most $N_h N_x N_y$ where N_h is the length of the window used in the interpolation. Thus, the total number of (complex) multiplications is given by $N_\omega N_a + N_\omega N_a \log_2 N_a + N_\omega N_a + N_x N_y (\log_2 N_x + \log_2 N_y) + N_h N_x N_y$. The terms are for the first phase multiplication, 1-D FFT, second phase multiplication, interpolation and 2-D IFFT, respectively. In GIM, the quantities given by (4), (6) and (9) can be precomputed because of their dependence only on the transmitted pulse and the data collection geometry. The computation of the multichannel deconvolution filter can be done off-line as well. Thus, the required number of (complex) multiplications, once the off-line computations have been completed, is $IN_t N_a + [(N_a I + M) N_a \log_2 N_a + M N_a I] + M N_y N_x$, corresponding to (5), (11) and (12), respectively. Here, N_t is the number of spatial samples in the x-direction for the range compressed return signal given in (2).

In the following simulations, the temporal center frequency of the radar signal was 10 GHz and the bandwidth was 32 MHz. The radar traveled 500 m along track and illuminated a scene area of 120 m by 500 m. Considering the sampling requirements, we let $N_t = 128$ and $N_a = 256$. After running GIM for a simulation with $N_x = N_y = 128$, we obtained I and M values and calculated $N_\omega = 6912$ which makes the number of computations for both algorithms equal. With that number of temporal frequency samples, the interpolation step in the $\omega - k$ algorithm is accurate [1].

Figure 3(a) shows the image reconstructed by GIM, where the actual locations of the simulated point targets are (0, 3000), (20, 3100), (40, 3200), (60, 3300), (80, 3400); all numbers are in meters. Notice that the target at (0, 3000) is at the center of the runway. For this simulation there was no measurement noise in the

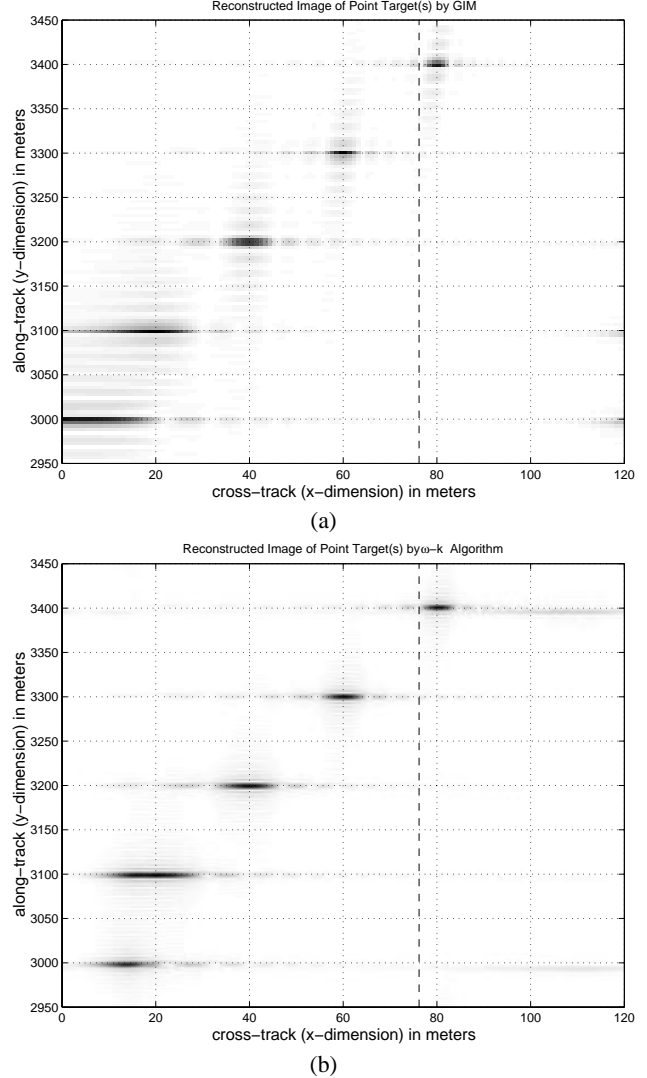


Fig. 3. Image of point targets reconstructed by (a) GIM, (b) $\omega - k$ algorithm. No noise.

return signal. The scene center is at (60, 3200), which corresponds to a squint angle of $\gamma_0 = 88.93^\circ$. The dashed line at $x = 76.2$ m is the edge of the FAA zone¹. The corresponding image obtained by the $\omega - k$ algorithm is given in Figure 3(b). In the $\omega - k$ reconstruction, the sidelobes are at least 12 dB below the mainlobe. Those for the GIM reconstruction are at least 13 dB below the mainlobe. The reason for the variety of target positions is that we wished to investigate the image reconstruction performance as a function of target location, especially in the cross-track direction. In both of the reconstructions, targets relatively far away from the center of the runway are reconstructed at their correct locations. For the target at the center of the runway, the $\omega - k$ reconstruction has a narrow mainlobe but it is shifted from its true location. In the GIM reconstruction, the mainlobe peak is located at $x = 0$

¹FAA regulations require that aircraft and vehicles maintain a distance of 76.2 m (250 ft) from the center of the runway when they do not have clearance to proceed to the runway.

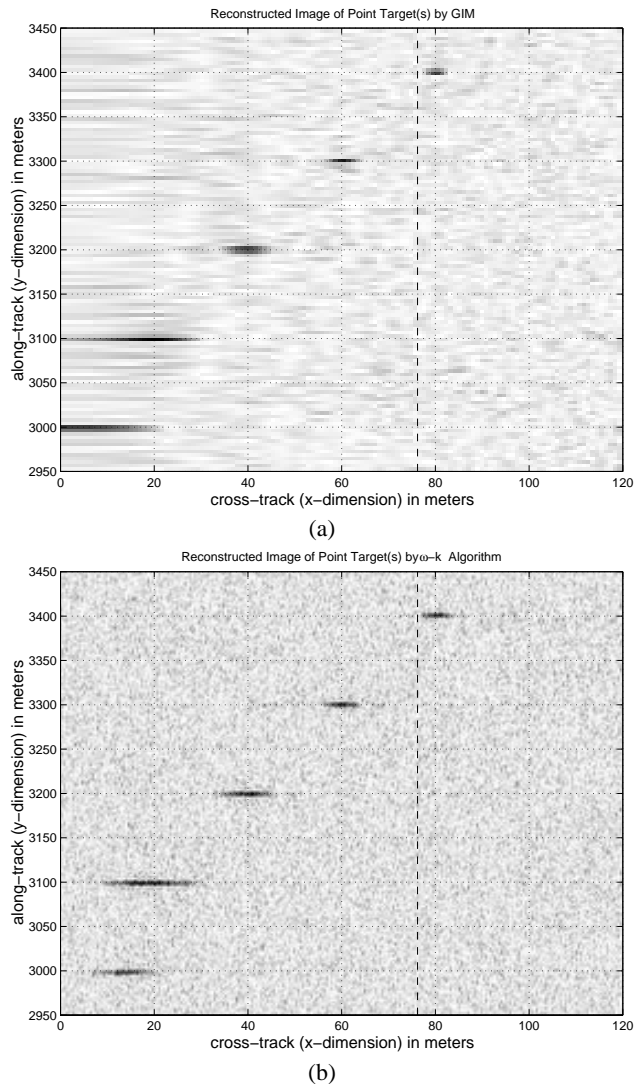


Fig. 4. Image of point targets reconstructed by (a) GIM for SNR=30 dB, (b) $\omega - k$ algorithm for SNR=40 dB.

but it is much wider; hence, it is not possible to detect the location accurately. However, in runway imaging, targets on or very close to the runway need not be imaged with high resolution. An indication of their existence in the FAA zone is sufficient, which occurs in Figure 3. We notice spreading of the energy of the target in the cross-track dimension, but this is expected since the range of observation angles for on-the-runway targets is exceedingly small.

In runway imaging, it is critical that targets inside the FAA zone not be imaged outside. For the reconstructions obtained by either of the methods, this is not a problem. Also, targets outside the FAA zone should not appear inside and cause a false alarm, which, of course, is a less hazardous case. From the simulations, it is seen that targets that are inside the FAA zone but not close to the runway center are accurately imaged. Objects outside the FAA safety zone will be imaged with even higher resolution, eliminating the possibility of a false alarm.

We also performed simulations for the case with measurement

noise in the return signal, assuming additive white Gaussian noise. Notice that for the noisy case, the equations (1), (2), (7) and (8) must be appended with an additive noise term. Figure 4(a) is a reconstruction by GIM for a 30 dB SNR. The weakest reconstructed target image has sidelobes that are about 9 dB below the mainlobe. The corresponding $\omega - k$ reconstruction is not shown since the targets were not identifiable in the image. However, for a less noisy case of 40 dB SNR, the reconstruction is shown in Figure 4(b). The weakest target has sidelobes that are about 8 dB lower than the mainlobe.

As seen from the above simulations, the $\omega - k$ algorithm and GIM produce comparable reconstructions for the noiseless case. Under the constraint that both methods use the same number of computations, interpolation in the $\omega - k$ algorithm is accurate enough so that no aberrations pertaining to the inaccuracies of the interpolation step occur. GIM is more robust to noise as seen from the simulations, which could be of value in some scenarios. Recall, however, that for GIM we did not factor in some computations that could be performed prior to data collection, off-line. If the geometry for data collection is not known a priori, then these additional computations must be performed on-line, which would greatly add to the complexity of GIM.

5. REFERENCES

- [1] Nail Çadallı and David C. Munson, Jr., "A simulation study of the $\omega - k$ SAR algorithm for the highly squinted case with application to runway imaging," in *Proc. IEEE Int. Conf. Acoust., Speech, Signal Processing*, Istanbul, Turkey, June 5-9, 2000.
- [2] Charles V. Jakowatz, Jr., Daniel E. Wahl, Paul H. Eichel, Dennis C. Ghiglia, and Paul A. Thompson, *Spotlight-Mode Synthetic Aperture Radar: A Signal Processing Approach*, Kluwer Academic Publishers, 1996.
- [3] Jung Ah C. Lee and David C. Munson, Jr., "Effect of a nonplanar wavefront in spotlight-mode synthetic aperture radar," in *Proc. IEEE Int. Conf. Image Processing*, Austin, TX, U.S.A., Nov. 13-16, 1994.
- [4] C. Cafforio, C. Prati, and F. Rocca, "SAR data focusing using seismic migration techniques," *IEEE Trans. Aerospace and Electronic Systems*, vol. 27, no. 2, pp. 194-207, March 1991.
- [5] Mehrdad Soumekh, "A system model and inversion for synthetic aperture radar imaging," *IEEE Trans. Image Processing*, vol. 1, pp. 64-76, Jan. 1992.
- [6] Orhan Arıkan, "Regularized inversion of a two-dimensional integral equation with application in borehole induction measurements," *Radio Science*, vol. 29, no. 3, pp. 519-538, May-June 1994.
- [7] Jung Ah C. Lee, Orhan Arıkan, and David C. Munson, Jr., "Formulation of a general imaging algorithm for high-resolution synthetic aperture radar," in *Proc. IEEE Int. Conf. Acoust., Speech, Signal Processing*, May 7-10 1996.
- [8] Jung Ah C. Lee and David C. Munson, Jr., "Runway imaging from an approaching aircraft using synthetic aperture radar," in *Proc. IEEE Int. Conf. Image Processing*, Sept. 16-19, 1996.